Cause and Amelioration of MRI-Induced Heating Through Medical Implant Lead Wires

Steven McCabe
Department of Engineering
The University of Waikato
Hamilton, New Zealand
Email: som1@students.waikato.ac.nz

Jonathan Scott
Department of Engineering
The University of Waikato
Hamilton, New Zealand
Email: jonathanscott@ieee.org

***Abstract*—The RF fields present in magnetic resonance imaging (MRI) scanners can induce hazardous heating in patients wearing medical implants. The inherent design and locale of deep brain stimulators (DBS) and spinal cord stimulators (SCS) make them particularly susceptible. We apply antenna concepts and use electromagnetic (EM) simulation to explain the phenomenon and anticipate its sensitivity to lead wire length. We anticipate that a DC resistance of less than $50\Omega/\mathrm{m}$ and an RF impedance of more than $1.23\mathrm{k}\Omega/\mathrm{m}$ would be required for a safe electrode for SCS use. We investigate the possibility of manipulating wire conductivity and diameter in order to use the skin depth effect to achieve a safe electrode. The effect of the thickness and permittivity of insulation surrounding the wires is explored.**

I. Introduction

Around 14,000 Spinal Cord Stimulation (SCS) systems are implanted in patients every year. Pacemakers and cochlear implants represent a more mature technology with some 3-million pacemakers and 300,000 cochlear implants in service in the world today. The newest implant technology is Deep Brain Stimulation (DBS), already approved for the treatment of Parkinson's disease, essential tremor, dystonia, epilepsy, and Obsessive-Compulsive Disorder (OCD) [1]. The number of implants can be expected to increase. Most of the patients wearing these technologies are contraindicated for MRI scans.

Most scientists are aware of the strong static magnetic field associated with an MRI machine. In actual fact, an MRI machine presents a hazard through three mechanisms, the static magnetic field; the low-frequency magnetic fields; and the enormous RF field [2]. The RF field produced in the older-generation $1.5\,\mathrm{T}$ MRI scanners has a frequency of $64\,\mathrm{MHz}$, whereas $3\,\mathrm{T}$ machines operate at $128\,\mathrm{MHz}$. A typical scan sequence can have RF pulses of up to $20\,\mathrm{kW}$ in power [3]. This can lead to significant heating of RF absorbers.

The International Commission on Non-Ionizing Radiation Protection (ICNIRP) recommends localised temperatures should remain below $38\,^{\circ}\mathrm{C}$ in the head, $39\,^{\circ}\mathrm{C}$ in the torso, and $40\,^{\circ}\mathrm{C}$ in the limbs [4]. In an MRI machine, the dielectric heating of a patient is monitored by the Specific Absorption Rate (SAR), the power absorption per unit mass of tissue. The SAR is typically averaged over the whole-body, whole-head, or $10\,\mathrm{g}$ of mass. There are claims in the literature that the measure is too coarse for detecting the power absorption near implants [5]. Highly concentrated electric fields near the small implant electrode can go undetected, leading to a higher than normal level of heating in this region.

Pacemakers are implanted close to the heart and have relatively short lead wires. This is also true of cochlear implants. SCS and DBS systems, on the other hand, have leads placed in the epidural cavity of the spine or deep in the skull, while the impulse generator and battery unit are normally placed in the chest cavity. In these systems, leads can easily exceed $600\,\mathrm{mm}$ in length. The leads are typically made of platinum wires running inside plastic polymer sheaths. Serious and fatal experience has shown that the RF heating risk rises with these longer leads [2], [5]. The MRI safety of implants has become a global issue and sites such as Shellock [6] are consulted throughout the world by MRI radiologists.

A spate of patents have appeared in the last decade supposedly addressing the issue of providing an MRI-safe electrode [3], [7]–[11]. Many seem to be conspicuously speculative in nature. Only one product has appeared [12]. It is rated for use only in 1.5T machines, and only with a restricted scanning protocol. The original patent appeared in 2010 [13].

In this work, we use Finite Element Method (FEM) simulation software to model the localised electric fields and temperature changes at the distal electrode of an implant lead wire as a function of length, in a $3\,\mathrm{T}$ MRI environment. We then explore various techniques that aim to reduce the level of RF heating. The first approach exploits the skin effect to maximise the AC resistance at RF, while maintaining a sufficiently lower resistance at the normal operational frequency of the neurostimulator. The second approach involves selection of suitable values for the insulation permittivity and thickness to reduce the characteristic impedance of the implant lead wire at RF. Verification of the improvements are provided by simulated results.

II. Simulation Models

The model, implemented in both two and three dimensions; is comprised of an insulated platinum wire (of variable length), embedded within a conductive phantom, inside of an RF antenna. The antenna operates at $128\,\mathrm{MHz}$, the RF frequency of a $3\,\mathrm{T}$ MRI machine. The three-dimensional model offers a more accurate representation of the MRI birdcage and rectangular phantom, and is used to assess the hazardous heating phenomenon. When the highest accuracy is not of critical importance, the computationally less demanding two-dimensional axisymmetric model is used.

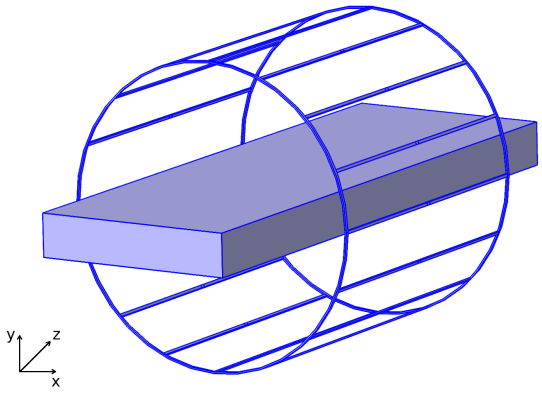

Fig. 1. Conductive phantom surrounded by a 16-rung RF birdcage antenna. A spherical perfectly matched layer surrounds the antenna (not shown).

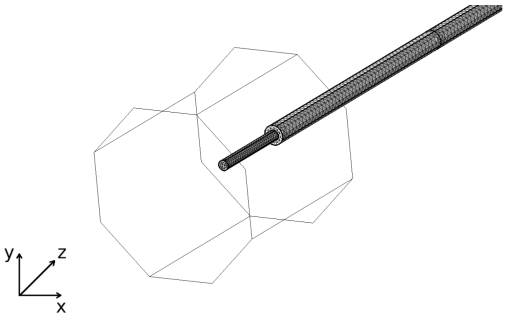

Fig. 2. The wire implant is comprised of a platinum conductor, 700 µm in diameter, surrounded by polyurethane insulation. 6 mm of insulation is missing from one end, representing the implant electrode.

A. Three-Dimensional Model

A list of the design parameters for the following components can be found in the appendix.

1) RF Birdcage Antenna: Modeled as a 16-rung birdcage antenna with a 0.6 m bore as shown in figure 1. The antenna generates circularly polarised electromagnetic (EM) waves with a free-space wavelength λ_0 of 2.34 m. Each rung is centre-driven by a sinusoidal signal[1]; differing by 22.5 ° in phase between adjacent rungs, with a total phase variation of 360 ° around the circumference of the antenna. All outgoing radiation is absorbed by a spherical perfectly matched layer (PML) surrounding the antenna.

2) Phantom: The parameters for the headless phantom model are set according to the ASTM F2182-11a international test standard [15] with the exception of the length parameter, which is doubled from 0.6 m to 1.2 m, to accommodate the testing of longer length wires. Blood perfusion is optional.

3) Implant: Modeled as a 700 µm platinum wire with polyurethane insulation as shown in figure 2. A small portion of the insulation is missing from one end, to imitate a distal electrode. A virtual cylindrical domain surrounding the distal electrode provides an enclosed boundary for subsequent extraction of the peak temperature. The opposite end of the wire is capped off with the polyurethane insulating material.

This is a simplified model of a more complex lead wire composed of multiple conductors, electrodes, and dielectrics.

[1]Practical birdcage antennas are typically fed between two points and require a multitude of tuning capacitors. For simulation purposes, simplification can be achieved by feeding an appropriate signal phase to the centre of each rung directly, eliminating the need for tuning capacitors [14].

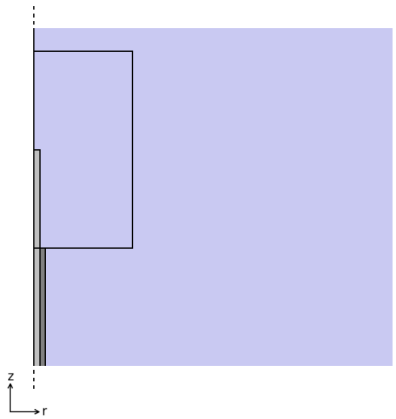

Fig. 3. Magnified view of the two-dimensional axisymmetric wire implant model with a virtual domain surrounding the distal electrode. The dashed lines represent the rotational axis.

B. Two-Dimensional Axisymmetric Model

Simulation times are significantly reduced for two-dimensional axisymmetric models (hours instead of days); however, only rotationally symmetric ones can be constructed in this space. A magnified view of the model showing the distal electrode is in figure 3. The MRI antenna (not shown) is simulated as a cylinder with a uniform current distribution. The radius and length are set to the same values as used in the three-dimensional model. Similarly, the phantom is modified to be cylindrical, with a radius of 0.21 m and a length of 1.2 m. The remaining relevant parameters are set to the same values listed for the three-dimensional model in the appendix.

C. Simulation Settings

For the subsequent simulations, the background Specific Absorption Rate[2] (SAR) was calibrated to a relatively modest level of 1 W/kg. The end time for temperature extraction was set to $t = 15$ min, the typical scan-time for MRI. Initial temperatures of the phantom and implant at $t = 0$ were 37 °C. Simulations were performed using the COMSOL Multiphysics 4.4 commercial software package.

III. Resonant Length

An implanted lead wire acts as a dipole antenna when exposed to the RF field from MRI. In this section, we explore the resonance phenomenon for the simple case of an uninsulated wire in a lossless medium, and then again for a lossy medium. Insulation is then added to the wire to replicate an implant lead wire and its effect is shown. The results are shown in terms of the average (mean) of the electric field enclosed within the virtual domain surrounding the distal end/electrode of the wire.

[2]The average SAR in the volume of the phantom, in the absence of the implant. Note that a non-conductive medium ($\sigma_P = 0$) will not absorb RF energy, and so the background SAR will consequently be zero. For the purpose of simulations, we apply the same signal amplitude to the antenna as we do for the lossy version.

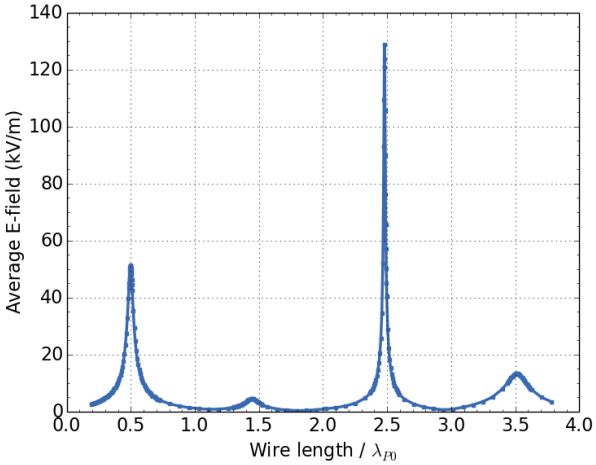

Fig. 4. Average E-field at one end of a 700 µm diameter bare wire for various lengths when the phantom is lossless ($\sigma = 0$).

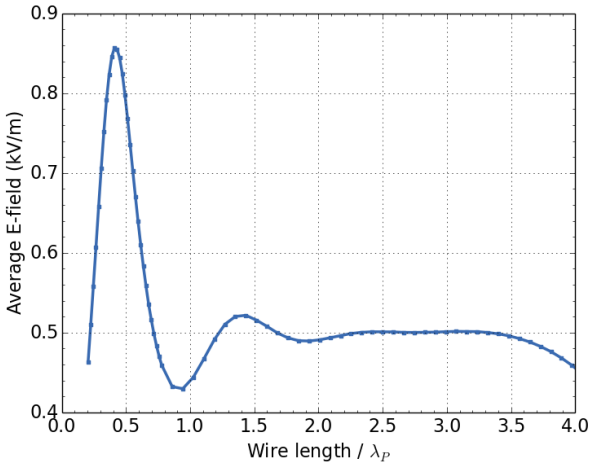

Fig. 5. Average E-field at one end of a 700 µm diameter bare wire for various lengths when the phantom is lossy ($\sigma = 0.47$ S/m).

A. Dipole Resonance

In a lossless medium ($\sigma = 0$), an ordinary dipole antenna will resonate when excited by an RF field when its length is approximately equal to an odd integer multiple of the half-wavelength: 0.5λ, 1.5λ, 2.5λ, $\cdots$. The wavelength of an EM wave in a lossless medium can be computed from

$$\lambda = \frac{2\pi}{\omega\sqrt{\mu\epsilon}} \tag{1}$$

where ω is the angular frequency, and μ and ϵ are the permeability and permittivity of the medium, respectively.

If the medium is conductive, the wave will compress. According to [16] the wavelength can be calculated from:

$$\lambda = \sqrt{\frac{8\pi^2}{\omega^2\mu\epsilon}} \cdot \left[\sqrt{1 + \left(\frac{\sigma}{\omega\epsilon}\right)^2} + 1\right]^{-1/2} \tag{2}$$

Furthermore, the induced antenna currents are not confined by the ends of the wire and are free to extend into the medium [17]. The antenna is effectively lengthened by the medium itself.

B. Lossless Phantom, Bare Wire

Suppose the phantom described in section II is the medium, but with zero conductivity ($\sigma_P = 0$), such that it is lossless. From equation 1, the wavelength inside of the phantom would be $\lambda_{P0} = 0.26$ m. A conductive wire within this region would be expected to resonate strongly when the length meets the aforementioned condition for resonance.

To verify this dipole antenna behavior, the two-dimensional axisymmetric model was simulated but with $\sigma_P = 0$ and no insulation on the platinum wire. The average electric field surrounding one end of the wire was extracted as a function of wire length. The location of the resonant frequencies correspond to that of a dipole antenna as is shown in figure 4. The average electric field in the space around the end of the wire maximises at resonance, the point when the end-to-end voltage on the dipole would be at maximum. Variation in the magnitude of each resonant peak can be attributed to the change in antenna impedance as the length is varied.

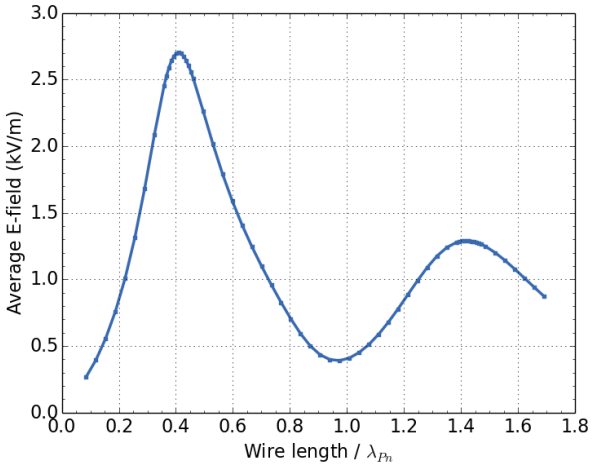

Fig. 6. Average E-field at the distal electrode of an insulated wire in a lossy phantom ($\sigma = 0.47$ S/m). The insulation covering the 700 µm diameter wire is 315 µm thick. The wire length is normalised to a wavelength of 0.59 m.

C. Lossy Phantom, Bare Wire

When the phantom has a finite conductivity of $\sigma = 0.47$ S/m, the international standard for MRI phantoms [15], the wavelength will shorten to $\lambda_P = 0.24$ m, according to equation 2. Simulation confirms a strong resonance at $0.41\lambda_P$, just shy of the half-wavelength as is shown in figure 5. Unlike the previous simulation where the phantom was non-conductive, induced currents have now entered the phantom from each end of the wire, changing its resonant behavior.

D. Lossy Phantom, Mostly-Insulated Wire

Simulation of the wire with insulation covering all but one end (the distal electrode) was performed. The average electric field near the distal electrode at various wire lengths is in figure 6. The length is normalised to

$$\lambda_{Pn} = 0.59\,\text{m}$$

such that the first resonant peak occurs at $0.41\lambda_{Pn}$. Not only has the insulation shifted the resonant frequency but it has also increased the electric field intensity at the first resonant peak threefold.

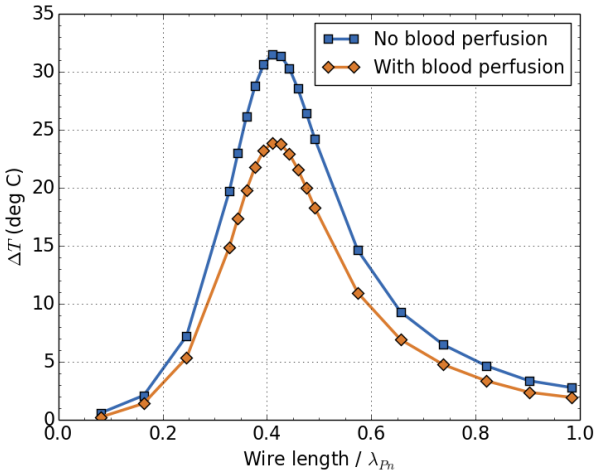

Fig. 7. The change in temperature ΔT near the distal electrode of the insulated wire after 15 minutes of simulated scanning. The insulation covering the 700 µm diameter wire is 315 µm thick. The length of the wire is normalised to a wavelength of 0.59 m.

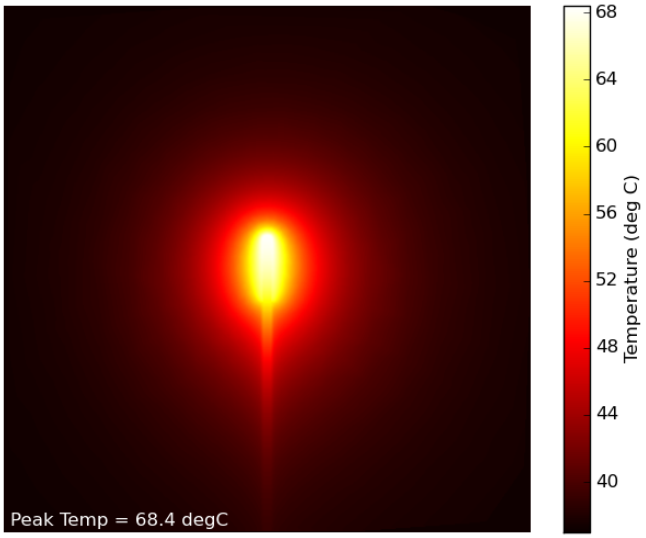

Fig. 8. The worst-case $T(x, z)$ at the distal electrode after 15 minutes of simulated scanning. The wire length was $0.41\lambda_{Pn}$ and blood perfusion was omitted. The initial temperature was 37 °C.

IV. RF Heating

The change in temperature $(T - 37\,^{\circ}\mathrm{C})$ at the distal electrode of the insulated wire after 15 min of MRI scanning, was simulated using the three-dimensional model from section II. The result is shown in figure 7. The x-axis is normalised to the wavelength of the electric field within the phantom, λ_{Pn}.

The exclusion of blood perfusion from the model provides an approximation of a worst-case scenario. At $0.41\lambda_{Pn}$ (0.24 m), normal body temperature is exceeded by almost 32 °C, well over the 2 °C limit for SCS. The peak temperature declines at longer wire lengths, similar to that of typical SCS and DBS lead wires, however, still exceeds specifications. A two-dimensional slice of the temperature T in the x-z plane at $y = 0$ is shown in figure 8, for when the wire length is $0.41\lambda_{Pn}$.

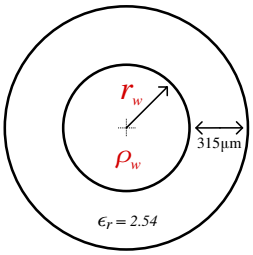

Fig. 9. The AC resistance of a conductive wire is a function of its radius and resistivity.

The model with blood perfusion offers more realistic values for temperature when there is sufficient blood flow around the distal electrode. Nevertheless, even with this heat loss, the peak temperatures reached are alarming. An implant comprising of an insulated wire(s) similar to the one simulated here, should be considered absolutely unsafe for MRI.

V. Method 1: Increase R_{AC}

A reduction in the heating of the tissue near the distal electrode could be achieved with the addition of a uniformly distributed AC resistance into the implant wire. The resistance would act to impede the flow of induced current (Ohm's law), leading to a reduction in power dissipation within the surrounding tissue of the distal electrode.

The proposed method for increasing the AC resistance of the wire is to select appropriate values for the radius r_w and resistivity ρ_w of the wire conductor such that the skin effect is maximised (see figure 9). In this section, we first determine the amount of AC resistance needed to reduce the heating to safe levels. Next, we discuss the skin effect and present equations for computing the AC resistance. Lastly, we determine values for r_w and ρ_w that will best reduce the heating effect.

A. Minimum R_{AC} Needed

To approximate the level of resistance necessary in the lead conductors of DBS and SCS systems, three-dimensional simulations of a hollowed out version of the implant wire were performed. The resistance was varied by controlling the resistivity of the metal. To ensure current uniformity, the resistivity was constrained to values such that the skin depth exceeded the thickness of the metal by at least 10 times. The AC resistance and the temperature change after 15 min as a function of the metal resistivity is shown in figure 10.

With 2 °C being the maximum level of heating allowed in the torso, it is apparent an SCS system would require at least 1.23 kΩ/m of AC resistance. Similarly, a maximum temperature change of 1 °C in the head, corresponds to a minimum AC resistance of 2.22 kΩ/m in DBS lead wires. Typically, neuro-stimulators are required to have no more than 50 Ω/m of DC resistance, such that the stimulation amplitude levels and battery life are not impaired.

B. Skin Effect

The AC current density J in a wire decays exponentially as a function of depth from the surface:

$$J = J_S e^{-d/\delta} \tag{3}$$

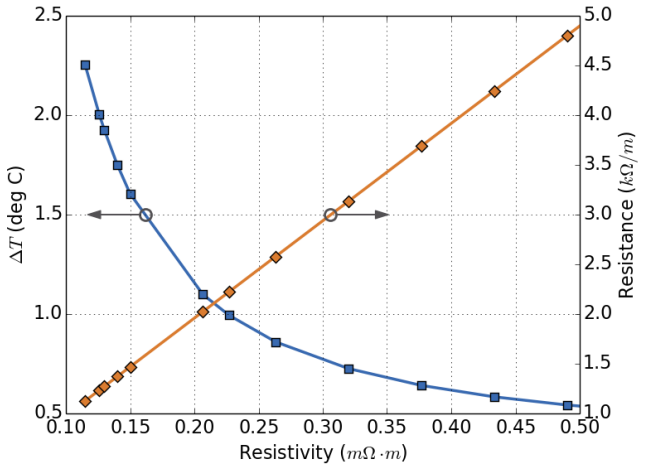

Fig. 10. The change in temperature ΔT near the distal electrode after 15 min of simulated scanning for a selected amount of uniform wire resistance. The linearity between the resistance and resistivity confirms that the skin depth is sufficiently larger than the metal thickness, such that the current is uniform.

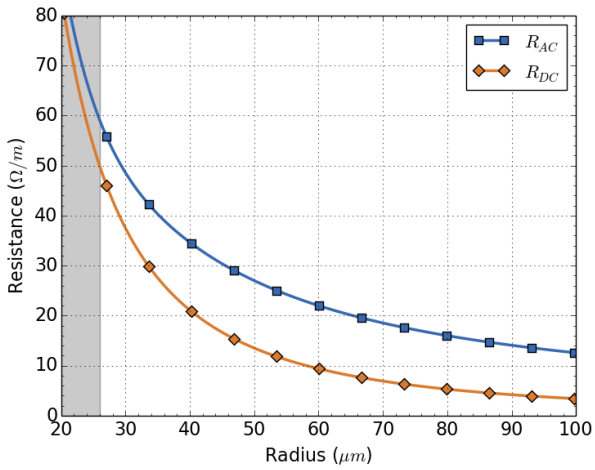

Fig. 11. The AC and DC resistance for a platinum wire over a range of radii. The shaded region is where the DC resistance exceeds 50 Ω/m limit.

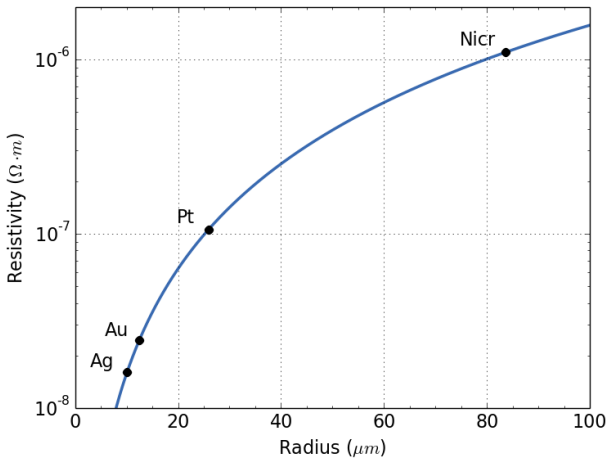

Fig. 12. Relationship between the wire resistivity and radius for a constant DC resistance of 50 Ω/m. The AC resistance is constant at 59.2 Ω/m over the entire range. Labels are shown for Silver (Ag), Gold (Au), Platinum (Pt), and Nichrome (Nicr).

where J_S is the current density at the surface, d is the depth from the surface, and δ is the skin depth. The skin depth is defined as the point where the current density has fallen to $e^{-1} \approx 37\%$. For highly conductive materials at RF, the skin depth can be sufficiently approximated to

$$\delta \approx \sqrt{\frac{2\rho}{\omega\mu}} \tag{4}$$

where ρ and μ are the resistivity and permeability of the conductor, respectively [18].

C. Resistance

A solid wire with uniform cross-sectional area, composed of a single homogenous material, has a resistance given by Pouillet's law:

$$R = \frac{\rho l}{A_{eff}} \tag{5}$$

where l is the length of the wire and A_{eff} is the effective cross-sectional area of the wire. For a cylindrical wire at DC, the current distribution is uniform and so $A_{eff} = \pi r^2$, where r is the radius of the wire. For AC, the current density is modified by the skin effect, where $A_{eff} \approx 2\pi r\delta$ for $r \gg \delta$.

To estimate the AC resistance when the wire radius is in the order of skin depths, a better approximation for the effective area is needed. The Modified Lorentzian Method [19] is a more accurate approximation even for conductors with radii much less than the skin depth. The effective area is calculated from

$$A_{eff} = \pi(2r\delta' - \delta'^2)(1 + y) \tag{6}$$

where

$$\delta' = \delta(1 - e^{-r/\delta})$$

$$y = \frac{0.189774}{(1 + 0.272481[z^{1.82938} - z^{-0.99457}]^2)^{1.0941}}$$

$$z = \frac{0.62006r}{\delta}$$

With equations 5 and 6, the AC and DC resistance was computed for a platinum wire ($\rho_w = 1.06 \times 10^{-7}\Omega m$) over a range of radii as shown in figure 11. Higher values of AC resistance are evident when the radius is small. However, the skin effect becomes less effective at smaller radii and the difference between the AC and DC resistance approaches zero. At the DC resistance limit of 50 Ω/m, the AC resistance is 59.2 Ω/m, with a radius of 26 µm. Through extrapolation of the simulated results in figure 10, this level of AC resistance will reduce ΔT to 27.6 °C at the worst-case length, an improvement of 14%.

For mechanical reliability, the radius of the wire may need to be larger than 26 µm. To achieve this without compromising on the AC resistance, the resistivity of the wire must be increased. The relationship between the radius and resistivity for a DC resistance of 50 Ω/m is shown in figure 12. The AC resistance is constant at 59.2 Ω/m over the entire range.

It is clear that at the specified RF frequency and DC resistance, the skin effect alone will not generate enough AC resistance to reduce heating to safe levels.

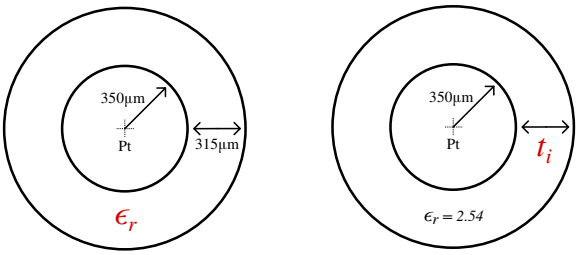

Fig. 13. The electric field and the heating at the distal electrode is a function of the insulation's (a) permittivity (b) and thickness.

VI. Method 2: Tune Wire Insulation Parameters

In section III, the insulation on the wire was shown to have an effect on the intensity of the electric field at the distal electrode. In this section we liken the implant lead wire to an RF transmission line and assess the electric field and heating of the distal electrode when the insulation's permittivity in figure 13(a) and thickness in figure 13(b) is varied.

Neglecting series resistance and shunt conductance, the characteristic impedance of a uniform coaxial transmission line can be calculated from

$$Z_0 = \frac{1}{2\pi}\sqrt{\frac{\mu}{\epsilon}} \cdot \ln\left(\frac{r_2}{r_1}\right) \tag{7}$$

where r_1 is the radius of the inner conductor, r_2 is the radius of the outer conductor, and μ and ϵ are the absolute permeability and permittivity of the dielectric material, respectively.

To some approximation, an implanted lead wire resembles a coaxial transmission line but with conductive tissue representing the outer cylindrical conductor [24]. Modification of the permittivity and thickness $(r_2 - r1)$ of the wire insulation will have a direct impact on its Z_0, and therefore, the amount of RF energy that is coupled to the implant lead wire.

A. Permittivity

Simulations of the two-dimensional model over a range of insulation permittivities yielded the result in figure 14. The wavelength in each sweep is normalised to:

$$\lambda_{P\epsilon_r} = \begin{cases} 0.59\,\text{m}, & \epsilon_r = 2.54 \\ 0.46\,\text{m}, & \epsilon_r = 5 \\ 0.37\,\text{m}, & \epsilon_r = 10 \\ 0.26\,\text{m}, & \epsilon_r = 80 \end{cases}$$

Due to long computation times, three-dimensional simulations of ΔT near the distal electrode at $t = 15\,\text{min}$ were performed only at the worst and best-case wire lengths. The values are overlaid on the same figure. Despite the considerable reduction in heating at higher permittivity values, the improvement is still not quite enough, even when ϵ_r has an impractical value of 80.

B. Thickness

A similar result can be found when sweeping the insulation thickness as shown in figure 15. The wavelength in each sweep

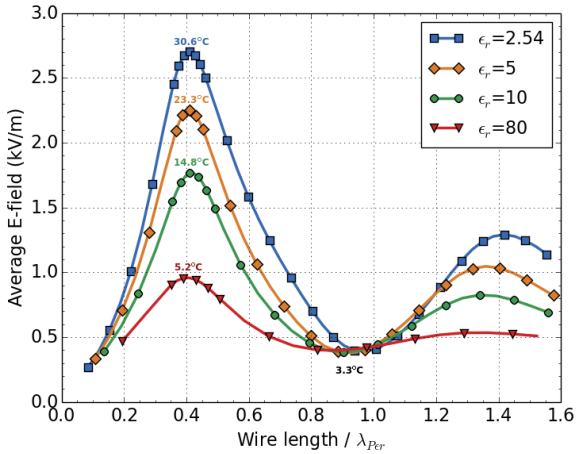

Fig. 14. Average E-field at the distal electrode for various insulation permittivities when $t_i = 315\,\mu\text{m}$. The overlaid values for ΔT were derived using the three-dimensional model. The length of the wire is normalised to stated values.

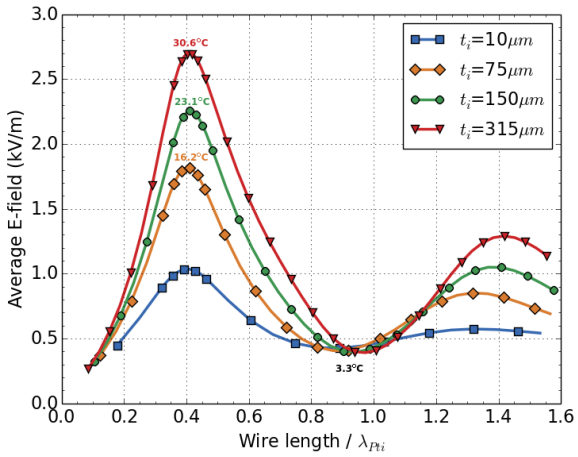

Fig. 15. Average E-field at the distal electrode for various thickness of insulation when $\epsilon_r = 2.54$. The overlaid values for ΔT were derived using the three-dimensional model. The length of the wire is normalised to stated values.

is normalised to:

$$\lambda_{Pt_i} = \begin{cases} 0.28\,\text{m}, & t_i = 10\,\mu\text{m} \\ 0.40\,\text{m}, & t_i = 75\,\mu\text{m} \\ 0.48\,\text{m}, & t_i = 150\,\mu\text{m} \\ 0.59\,\text{m}, & t_i = 315\,\mu\text{m} \end{cases}$$

It can be seen that by decreasing the thickness of the insulation, heating can be reduced significantly. Again, modifying the thickness parameter alone is unlikely to reduce the heating to safe levels, especially when the thickness becomes impractically small.

VII. Conclusion

When an insulated wire of sufficient length is embedded within conductive tissue and subject to MRI, it essentially becomes a dipole antenna, absorbing RF energy and heating the distal electrode and surrounding tissue to unacceptable levels. We have shown that a resistance of $1.23\,\text{k}\Omega/\text{m}$ is sufficient to reduce distal heating to a safe level for SCS, where implant manufacturers would like a resistance of less

than $50\,\Omega$/m for power consumption reasons. We have also shown that it is impractical to rely on the skin effect to give this combination of resistances in a 3 T machine. Either a thin or very high dielectric insulation could significantly reduce distal heating but may not be viable through considerations of reliability and patient safety. It may be possible that a combination of these design solutions could achieve an MRI-safe neuro-stimulator lead wire.

ACKNOWLEDGEMENT

We would like to thank the Waikato Medical Research Foundation (WMRF) for funding. We also acknowledge WaikatoLink and KiwiNet for their valuable support. Thanks are due to the University of Waikato for their research scholarship.

APPENDIX

TABLE I. 3D MODEL PARAMETERS.

	Parameter	Assignment
Birdcage antenna [14]	r_b	0.3 m
	l_b	0.6 m
	Material	PEC
	N_{rung}	16
	w_{rung}	6 mm
	f	128 MHz
	$\Delta\phi$	$22.5\,^\circ$
Phantom [15], [20]	w_p	0.42 m
	l_p	1.2 m
	h_p	0.09 m
	(x_p, y_p, z_p)	Centered within antenna
	ϵ_{rp}	80
	μ_{rp}	1
	σ_p (optional)	0.47 S/m
	ρ_p	1000 kg/m^3
	C_{pp}	4150 J/(kg K)
	k_p	0.6 W/mK
Blood perfusion (optional) [21]	T_b	$37\,^\circ$C
	C_b	4180 J/(kg K)
	ω_b	6.4×10^{-3} (1/s)
	ρ_b	1000 kg/m^3
	Q_{met}	0 W/m^3
Implant wire[3] **(Platinum)** [2]	r_w	0.35 mm
	l_w	Variable
	(x_w, y_w, z_w)	(0.16 m, 0, 0)
	Bound. mesh t_{bw}	$\delta_{Pt}/4$
	Bound. mesh N_{bw}	20
Implant insulation (optional) [2], [22]	t_i	0.315 mm
	l_i	$l_w - 6$ mm
	ϵ_{ri}	2.54
	μ_{ri}	1
	σ_i	4.7×10^{-4} S/m
	c_{pi}	1760 J/(kg K)
Virtual domain	r_v	6 mm
	l_v	12 mm
	(x_v, y_v, z_v)	Centered about tip face
Perfectly matched layer (PML) [23]	Inner radius	$2.0\lambda_0/4$
	Outer radius	$2.5\lambda_0/4$

REFERENCES

[1] "Medtronic Deep Brain Stimulation (DBS): The Road to the 100,000th Implant" Poster, Medtronic, Inc. 2012. http://multimediacapsule.thomsonone.com/file/download/1616/RelatedDocuments/673 retrieved Sept 2014.

[2] J. A. Nyenhuis, P. Sung-Min, R. Kamondetdacha, A. Amjad, F. G. Shellock and A. R. Rezai "MRI and Implanted Medical Devices: Basic Interactions With an Emphasis on Heating", IEEE Transactions on Device and Materials Reliability, vol.5, no.3, pp.467-480, Sept. 2005.

[3] The skin depth of platinum at 128 MHz is 14.4 µm.

[3] J. M. Olsen, S. L. Bolea, G. A. Hrdlicka, C. D. Wahlstrand, and T. B. Hoegh, "Lead Electrode for Use in an MRI-Safe Implantable Medical Device", International patent number *WO 2006/093685 A1*, Sept, 2006.

[4] "ICNIRP Statement on: Medical Magnetic Resonance (MR) Procedures: Protection of Patients", International Commission on Non-Ionizing Radiation Protection (ICNIRP), *Health Phys.*, vol. 87 no. 2, pp. 197-216, Aug. 2004.

[5] L. M. Angelone, J. Ahveninen, J. W. Belliveau and G. Bonmassar, "Analysis of the Role of Lead Resistivity in Specific Absorption Rate for Deep Brain Stimulator Leads at 3T MRI", IEEE Transactions on Medical Imaging, vol.29, no.4, pp.1029-1038, April 2010.

[6] "MRISAFETY.COM, Your Information Resource for MRI Safety, Bioeffects, & Patient Management", http://www.mrisafety.com/ retrieved Sept 2014.

[7] C. D. Wahlstrand and T. B. Hoegh, "Electrode for Use in an MRI-Safe Implantable Medical Device", European patent number *EP 1 742 701 B1*, Aug, 2010.

[8] C. D. Wahlstrand, G. A. Hrdlicka, R. M. Skime, P. Przybszewski, and T. E. Cross, "Energy Shunt for Producing an MRI-Safe Implantable Medical Device", International patent number *WO 2005/030322 A1*, Apr, 2005.

[9] B. A. Tranchina, "Method for Fabricating a Stimulation Lead to Reduce MRI Heating", US patent number *8,601,672 B2*, Dec, 2013.

[10] G. Bonmassar and E. Eskandar, "MRI Compatible Leads for a Deep Brain Stimulation System", International patent number *WO2014055737 A1*, Apr, 2014.

[11] C. D. Wahlstrand, R. M. Skime, G. A. Hrdlicka, J. M. Olsen, and S. L. Bolea, "MRI-Safe Implantable Medical Device", US patent number *8,620,453 B2*, Dec, 2013.

[12] *MRI and SCS, SureScan System* Medtronic, USA, Implant Manual, 2013. http://www.mrisurescan.com/au/for-radiologists/spinal-cord-stimulators/mri-and-scs/index.htm#tab2 retrieved Aug 2014.

[13] T. B. Hoegh, S. L. Bolea, C. D. Wahlstrand, G. A. Hrdlicka, and J. M. Olsen, "Lead Electrode for Use in an MRI-Safe Implantable Medical Device", European patent number *EP 1 740 260 B1*, Aug, 2010.

[14] O. Talcoth, T. Rylander, "Electromagnetic modeling of pacemaker lead heating during MRI", Technical Report, Chalmers University of Technology, Sweden, 2011.

[15] *F2182-11a Standard Test Method for Measurement of Radio Frequency Induced Heating On or Near Passive Implants During Magnetic Resonance Imaging,* ASTM International, West Conshohocken, PA, USA, 2010.

[16] R. K. Shevgaonkar, "Electromagnetic Waves", *Tata McGraw-Hill*, pp. 175, 2006.

[17] J. E. Brown, "Radiofrequency Heating Near Medical Devices in Magnetic Resonance Imaging", PhD thesis, Univ. of Florida, May 2012.

[18] S. Ramo, J. R. Whinnery and T. Van Duzer, *Fields and Waves in Communication Electronics, Second Edition*, John Wiley & Sons, Inc, pp. 147-150, 1984.

[19] D. W. Knight, "Practical Continuous Functions For the Internal Impedance of Solid Cylindrical Conductors", Apr 2013.

[20] S. A. Mohsin, N. M. Sheikh, and U. Saeed, "MRI Induced Heating of Deep Brain Stimulation Leads: Effect of the Air-Tissue Interface", Progress in Electromagnetics Research, PIER 83 pp.81-91, 2008.

[21] "Hepatic Tumor Ablation", Comsol Multiphysics Model Example, Model ID: 497. http://www.comsol.com/model/hepatic-tumor-ablation-497 retrieved Sept 2014.

[22] N. Gallagher, C. E. Fear, I. A. Byrd, and E. J. Vigmond, "Contact Geometry Affects Lesion Formation in Radio-Frequency Cardiac Catheter Ablation", PLOS ONE Journal, vol.8, no.9, pp.1-10, Sept 2013.

[23] "Modeling a Dipole Antenna", Comsol Multiphysics Model Example, Model ID: 8715. http://www.comsol.com/model/modeling-a-dipole-antenna-8715 retrieved Sept 2014.

[24] R. W. P. King and G. S. Smith, "Antennas in matter: fundamentals, theory, and applications", *The MIT Press*, Cambridge, MA, 1981.